ISME

Iranian Journal of Mechanical Engineering
The Iranian Society of Mechanical Engineers
Research Paper

DOI: 10.30506/JMEE.2022.543599.1278
DOR: 20.1001.1.16059727.2022.23.2.5.4

H. Vahidi[*]
Ph.D. Candidate

M. Shahgholi[†]
Associate Professor

A. Rahmani Hanzaki[‡]
Associate Professor

A. Mohamadi[§]
Ph.D.

Stability Analysis of an Axially Moving Thin Wall Conical Shells Made of Shape Memory alloy

The current paper presents the free vibration characteristic of axially moving conical shells made of shape memory alloy based on Donnell's shell theory. The material behavior is simulated based on the Boyd-Lagoudas model. By applying the suitable airy function, the strain compatibility equation, and the Galerkin method, two sets of equations of motion are obtained. The compatibility equation is solved by using the steady-state form of equations and employing the suitable flexural mode shape concerning radial displacement. The effects of moving in the axial direction and using the SMA are investigated with the aid of the frequency responses curves. The phase transformation would decrease the quantity of the critical velocity. The results have been evaluated by means of the available data.

Keywords: Conical shell, Axially moving, Stability, Shape memory alloy

1 Introduction

Axially moving Conical shells has many applications in such as medical equipment, aerospace industries, marine industries, military equipment. This type of movement causes large deformation in the transverse direction compared with the thickness of the shell. The Multiple-scale method analysis can help us to study more detail. For motion both axial and circumferential, the governing equation is more implicated than separately. An internal variable approach is used to derive a constitute relation for shape memory material without the assumption of constant material function by Brinson [1]. Paiva and Savi presented an overview of the thermomechanical behavior of shape memory alloy and finally presented five phenomenological theories. These models capture the general thermodynamical behavior of shape memory alloy, characterized by pseudo elastics, shape memory effect, phase transformation due to temperature variation, and internal subloops due to incomplete phase transformation [2].

[*] Ph.D. Candidate, Faculty of Mechanical Engineering, Shahid Rajaee Teacher Training University, Tehran, Iran
[†] Corresponding Author, Associate Professor, Faculty of Mechanical Engineering, Shahid Rajaee Teacher Training University, Tehran, Iran
[‡] Associate Professor, Faculty of Mechanical Engineering, Shahid Rajaee Teacher Training University, Tehran, Iran
[§] Ph.D., Faculty of Mechanical Engineering, Shahid Rajaee Teacher Training University, Tehran, Iran

Receive: 2021/11/24 Accepted: 2022/07/24

To vibration reduction of the primary system subjected to external excitation a tuned vibration absorber (TVA) is well established by Savi, De Paula [3]. The application of SMAs spans a wide variety of industrial sectors such as aerospace, automotive, biomedical, and oil exploration. Lagoudas provide insights into the history of SMAs, their properties, their microstructural behavior, and varied industrial applications [4]. A model proposed by Tanaka and Tanaka, Kobayashi assumes exponential hardening functions for SMA materials [5,6]. the cosine model proposed by Liang and Rogers [7]. A series of papers by Bo and Lagoudas studied the cyclic behavior of SMAs in one-dimensional [8-11]. The internal variables are the total martensite volume fraction and reoriented martensite volume fraction. Leclercq and Lexcellent use two internal variables to allow modeling of both detwinned and self-accommodated martensite [12]. The exponential function is used to describe that. both temperature and stresses induced are considered to formulate a single transformation function with kinematic hardening [13]. The free vibrations of conical shells have been studied by many researchers using various methods. Civalek employed the discrete singular convolution method to analyze the vibration of a rotating conical shell [14]. Chen and Dai investigated the dynamic stability using the harmonic balance method. In this paper, the dynamic properties of the rotating conical shell are studied by considering the internal coupling of high and low-order modalities, which is analyzed by the harmonic balance method [15]. Sofiyev investigated the non-linear vibration of truncated conical shells made of functionally graded materials (FGMs) subjected to uniform axial compressive loading and analyzed by Using the superposition, the Galerkin, and harmonic balance methods, the modified Donnell type non-linear stability equation of motion, and the compatibility equation [16]. Chen, Zhao analyzed the vibration of high-speed rotating shells with an analytical solution [17]. Mohamadi, Shahgholi investigated linear free vibration of axially moving thin circular cylindrical shells to achieve natural frequency. The multiple scale method was employed, and several types of instability are discussed. These three articles would be references to validate this work [18]. A study based on the first-approximation love theory, and the Galerkin procedure done by Hua, determined the frequency of truncated circular orthotropic conical shells concerning axial spinning [19-21]. Abolhassanpour, Ashenai Ghasemi investigated linear free vibration of axially moving thin wall truncated conical shells by using the multiple scale method [22]. Nonlinear response of rotating circular cylindrical shells with the precession of vibrating shape subjected to a harmonic excitation is done by Wang, Guo [23]. Sarkheil and Foumani investigated the vibrations of a truncated conical shell under rotating conditions with considering Coriolis and centrifugal force and the initial Hoop tension of rotation [24]. In 2019 Wang, Ding review the vibration of an axially moving hyperelastic beam under simply supported conditions [25]. Sofiyev and Pancar investigated the instability of truncated conical shells by Bolotin's method [26]. Shin, Chung investigated the vibration of the axially moving membrane. The related equation is derived by employing the extended Hamilton principle and discretized by the Galerkin method to compute the natural frequency and the mode shape [27]. Najafov, Sofiyev presented axially compressed three-layered truncated conical shells. The modified Donnell-type dynamic stability and compatibility equation are derived and solved by the Galerkin method eventually, and dimensionless frequency parameters, and dimensionless critical axial loads are derived in this work [28]. Anh and Duc studied the vibration of composite truncated conical shells surrounded by an elastic medium in a thermal environment by using a semi-analytical approach and the Galerkin method [29]. Kerboua, Lakis studied the behavior of anisotropic truncated conical shells conveying fluid [30]. The vibration and stability of carbon nanotube reinforced composite truncated conical shells are studied by Sofiyev [31]. an analytical solution is employed to obtain the frequency and critical axial load. the stability of a conical shell constrained the acting loads in the form of longitudinal compressive force and lateral pressure in an elastic-plastic domain is considered by Shokrollahi [32]. Avey, Fantuzzi studied the thermoelastic stability of carbon

nanotube composite conical shells with two different boundary value problems [33]. The buckling of generally laminated conical shells having thickness variations under axial compression is investigated by Kazemi, Kouchakzadeh [34]. The transient dynamic response of the composite conical shell with simply supported boundary conditions under the lateral impact load is investigated by Zamani, Davar [35]. SMA innovation execution within the aerospace industry has spanned the areas of fixed-wing aircraft, marine, rotorcraft, space craft and work in all these areas is still advancing. Temperature and stresses of body and cape of high-speed flight vehicles due to aerodynamic resistance significantly rise [36].
The main aim of this study first is the issue of the problem which is axial movement conical shell made of SMA along the axis which has many applications and so far, no study has been done in this regard. second, the application of the method of choosing a suitable solution like the multiple-scale method and the flexural mode shape by using some suitable relations that are expressed by researchers. Using the convenient theory, and convenient hypothesis, Donnell-Mushtari shell theory to solve the problem. The compatibility equation is solved based on the initial and boundary conditions. Afterward, the nonhomogeneous partial differential motion equation in the radial direction is districted into a set of ordinary differential equations. Based on the generalized coordinates with the aid of the Galerkin method, the frequency response, and the bifurcation diagrams the behavior of the systems in various axial velocities along its axis be predicted.

2 Constitutive relation

In this paper, the relations proposed in [4] based on the Gibbs free energy as a function of stress tensor (σ), temperature (T), martensite fraction (η), and transformation strain tensor (ε^t) are utilized as:

$$G(\sigma,T,\eta,\varepsilon^t) = -\frac{1}{2}\sigma:S:\sigma - \frac{1}{\rho}\sigma:[\alpha(T-T_0)+\varepsilon^t] + c\left[(T-T_0) - TLn\left(\frac{T}{T_0}\right)\right] - s_0T + u_0 + \frac{1}{\rho}f(\eta) \tag{1}$$

In which (:) signifies the Frobenius inner product of two tensors while, A and M, refer to austenite and martensite states, and 0 implies the initial values, respectively. Furthermore, S, α, c, s_0 and u_0 are the effective compliance tensor, thermal expansion tensor, specific heat capacity, entropy, specific and internal energy correspondingly. The parameters can be expressed as follows:

$$S(\eta) = S^A + \eta(S^M - S^A) \tag{2}$$

$$c(\eta) = c^A + \eta(c^M - c^A) \tag{3}$$

$$s_0(\eta) = {s_0}^A + \eta({s_0}^M - {s_0}^A) \tag{4}$$

$$u_0(\eta) = {u_0}^A + \eta({u_0}^M - {u_0}^A) \tag{5}$$

$$\alpha(\eta) = \alpha^A + \eta(\alpha^M - \alpha^A) \tag{7}$$

In addition, $f(\eta)$ is the transformation hardening function, which is expressed as:

$$f(\eta)=\begin{cases}\frac{1}{2}\rho b^{M}\eta^{2}+(\mu_1+\mu_2)\eta, & \dot{\eta}>0\\ \frac{1}{2}\rho b^{A}\eta^{2}+(\mu_1-\mu_2)\eta, & \dot{\eta}<0\end{cases} \tag{6}$$

Since in eq. (7), $\dot{\eta}$ is the time rate of the martensite fraction, $\dot{\eta}>0$ which means that the fraction of martensite is increasing. In other words, the material phase is changing from austenite to martensite (A → M), and vice versa for $\dot{\eta}<0$ (as is seen in Fig. (1)). The other parameters of eq. (7) are expressed in Appendix A, namely, equations (A-1) and (A-2).
By combining the first and the second Laws of thermodynamics, the Clausius-Plank inequality is derived, which is:

$$-\rho\dot{G}-\dot{\sigma}:\varepsilon-\rho s\dot{T}\geq 0 \tag{8}$$

Where s and ε are entropy and strain tensor and are obtained from eqs. (9) and (10).

$$\varepsilon=-\rho\frac{\partial G}{\partial\sigma}=S:\sigma+\alpha(T-T_0)+\varepsilon^{t};\ \ \varepsilon^{t}=Hsgn(\sigma)\eta \tag{9}$$

$$s=-\frac{\partial G}{\partial T}=\frac{1}{\rho}\sigma:\alpha+CLn\left(\frac{T}{T_0}\right)+s_0 \tag{10}$$

By substituting s and ε from eqs. (9) and (10) into eq. (8), the Clausius-Plank inequality will be:

$$\left(-\rho\frac{\partial G}{\partial\varepsilon^{t}}\right):\dot{\varepsilon}^{t}+\left(-\frac{\partial G}{\partial\eta}\right)\dot{\eta}\geq 0\Longrightarrow\sigma:\dot{\varepsilon}^{t}+(-\rho\frac{\partial G}{\partial\eta})\dot{\eta}\geq 0 \tag{11}$$

The relation between the martensitic fraction volume and the evolution of transformation strain is [4],[37]:

$$\dot{\varepsilon}^{t}=\Lambda\dot{\eta} \tag{12}$$

Equation (12) is called the flow rule which Λ is a transformation tensor and is expressed in Appendix A, equations (A-3) to (A-5):
By replacing $\dot{\varepsilon}^{t}$from eq. (12) into Eq. (11), the Clausius-Plank inequality is rewritten as:

$$(\sigma:\Lambda-\rho\frac{\partial G}{\partial\eta})\dot{\eta}=\psi\dot{\eta}\geq 0 \tag{13}$$

Which ψ is the general thermodynamic force and can be expressed as:

$$\psi(\sigma,T,\eta)=\sigma:\Lambda+\frac{1}{2}\sigma:\Delta S:\sigma+\sigma:\Delta\alpha(T-T_0)-\rho\Delta c\begin{bmatrix}(T-T_0)-TLn\\ \left(\frac{T}{T_0}\right)\end{bmatrix}+\rho\Delta s_0T-\rho\Delta u_0-\frac{\partial f}{\partial\eta} \tag{14}$$

It should be noted that ψ is the function of stress and temperature so, the phase transformation will occur whenever this force reaches a critical value. For the forward martensite transformation, the threshold value of function ψ is shown by Y. Also, for the backward martensite transformation, the threshold of function ψ assumed to be $-Y$. The critical value, i.e., Y, is a quadratic polynomial hardening function and expressed in Appendix A, eq. (A-6). The transformation function (ϕ) is introduced as follows [4],[37]:

$$\phi = \begin{cases} \psi - Y, & \dot{\eta} > 0 \\ -\psi - Y, & \dot{\eta} < 0 \end{cases} \; ; \; Kuhn$$
$$- Tuker\ condition \begin{cases} \dot{\eta} \geq 0, & \phi(\sigma, T, \varepsilon) = \psi - Y \leq 0 \\ \dot{\eta} \leq 0, & \phi(\sigma, T, \varepsilon) = -\psi - Y \leq 0 \end{cases} \quad (15)$$

During both sides transformation ϕ =0, while for martensite ϕ <0 and $\dot{\eta} = 0$. This situation is called Kuhn-Tuker conditions, which are defined for both forward and backward transformations. The material phase transformation occurs when the martensite fraction is between zero and one ($0 \leq \eta \leq 1$). While, 0 indicates that the material is fully austenite, and 1 specifies that the material is fully martensite.

The algorithm of Fig. (1) shows an iterative correction methodology in which the internal variable, i.e., η, ε^t can be obtained at each step for the given strain. For the first step, a set of initial values is guessed. The iteration is continued until the transformation criterion, namely, $\emptyset \leq 0$ is satisfied. In the next steps, the converged internal variables of the previous step are used as the initial guesses. The procedure is continued until the transient phase is completed meaning that $\eta = 1$. The other internal required parameters are expressed in Appendix A, equations (A-7) to (A-12).

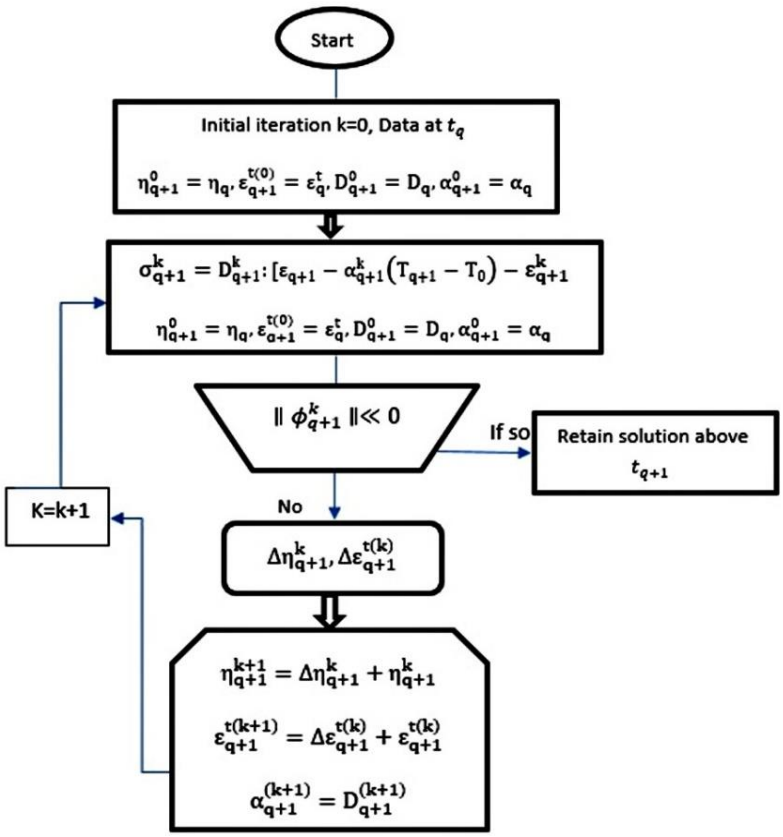

Figure 1 The iteration method chart for SMA [38]

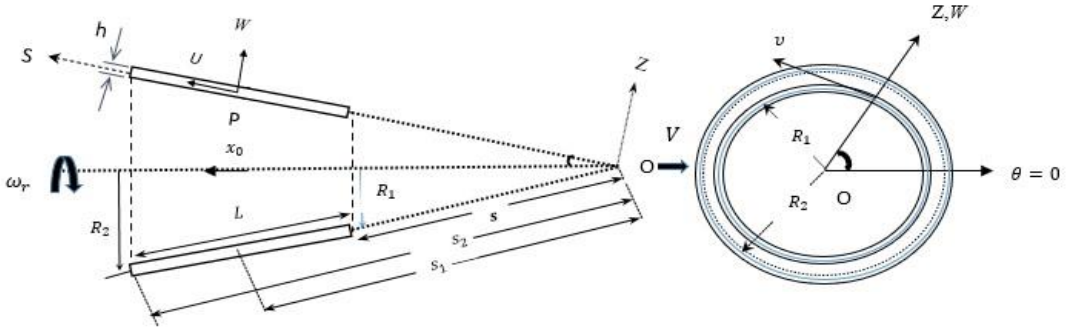

Figure 2 Geometry of the truncated conical shell

3 Formulations

Figure (2) shows a truncated cone that rotates around its longitudinal axis at speed (Ω), axial speed (V) where α is the angle of the cone, s, θ are the coordinates of the cantilever, $R_1, R_2$are the radius of both two ends, L is the length of the cone, S_1, S_2 are the distance between cone vertex and the middle and end of cone and h is the thickness of the cone. The reference surface for the rotation is taken to be at the middle surface of the cone and orthogonal references are fixed at the end as shown in the figure. Deformations are defined by u, v, and w in the meridional s, circumferential θ and normal z directions, respectively.
The following introduces the deformation component based on the classical shell theory [39]:

$$\begin{bmatrix} \varepsilon_s \\ \varepsilon_\theta \\ \varepsilon_{s\theta} \end{bmatrix} = \begin{bmatrix} \varepsilon_s^0 \\ \varepsilon_\theta^0 \\ \varepsilon_{s\theta}^0 \end{bmatrix} + Z \begin{bmatrix} K_s \\ K_\theta \\ K_{s\theta} \end{bmatrix} \tag{16}$$

Where, $\varepsilon_s^0, \varepsilon_\theta^0$ are the normal strain along with s and θ direction and $\varepsilon_{s\theta}^0$ is the shear strain at the middle surface of the cone. K_s, K_θ are the change in curative and $K_{s\theta}$ is the twist of the cone which are defined by Donnell-Mushtari shell theory assumes the following relationship [40]:

$$\varepsilon_s^0 = \frac{\partial u}{\partial s} \tag{17}$$

$$\varepsilon_\theta^0 = \frac{1}{s}\frac{\partial v}{\partial \varphi} + \frac{u}{s} - \frac{w\cot(\alpha)}{s} \tag{18}$$

$$\varepsilon_{s\theta}^0 = \frac{1}{s}\frac{\partial u}{\partial \varphi} + \frac{\partial v}{\partial s} - \frac{v}{s} \tag{19}$$

$$K_s = -\frac{\partial^2 w}{\partial s^2} \tag{20}$$

$$K_\theta = -\left(\frac{1}{s^2}\frac{\partial^2 w}{\partial \varphi^2} + \frac{1}{s}\frac{\partial w}{\partial s}\right) \tag{21}$$

$$K_{s\theta} = -\left(\frac{1}{s}\frac{\partial^2 w}{\partial s \partial \varphi} - \frac{1}{s^2}\frac{\partial w}{\partial \varphi}\right) \tag{22}$$

E, μ is the Young modulus, and Poisson's ratio, respectively. The force and moment components are achieved by integrating the stress components.

$$(N_s, N_\theta, N_{s\theta}) = \int_{-\frac{h}{2}}^{\frac{h}{2}} (\sigma_s, \sigma_\theta, \sigma_{s\theta}) dz \tag{23}$$

$$(M_s, M_\theta, M_{s\theta}) = \int_{-\frac{h}{2}}^{\frac{h}{2}} (\sigma_s, \sigma_\theta, \sigma_{s\theta}) z dz \tag{24}$$

3.1 Hamilton principle

In this work, the governing equation is derived from Hamilton's principle:

$$\int_0^{\mathrm{t}} (\delta \mathrm{T} - \delta \mathrm{U}) \mathrm{dt} = 0 \tag{25}$$

Where δK, δU are virtual kinetic energy, and virtual strain energy. The virtual kinetic energy obtained using the Love hypothesis is as follows:

$$\mathrm{U} = \frac{1}{2} \int_0^L \int_0^{2\pi} \int_{-\frac{h}{2}}^{\frac{h}{2}} (\sigma_s \varepsilon_s + \sigma_\theta \varepsilon_\theta + \tau_{s\theta} \varepsilon_{s\theta}) R dz d\theta ds \tag{26}$$

$$\mathrm{T} = \frac{1}{2} \int_0^L \int_0^{2\pi} \int_{-\frac{h}{2}}^{\frac{h}{2}} (\dot{u}^2 + \dot{v}^2 + \dot{w}^2) R dz d\theta ds \tag{27}$$

Finally, by employing the simplification of the Donnell shell theory assumption and using the equation (25), integrating the terms by part and using the SMA constitute relation, yield the equation of motion of axially moving and rotating truncated conical shells as:

$$\begin{aligned} &\frac{\partial \mathrm{N_s}}{\partial \mathrm{s}} + \frac{\partial \mathrm{N_{s\theta}}}{\partial \varphi} + \frac{N_s - N_\theta}{\mathrm{s}} - A_1 h \left[(1-\upsilon) \frac{\partial \varepsilon_{11}^t}{\partial x} + \upsilon \frac{\partial \varepsilon_{22}^t}{\partial x} + \upsilon \frac{\partial \varepsilon_{33}^t}{\partial x} + (1-2\upsilon) \frac{\partial \varepsilon_{12}^t}{\partial y} \right] \\ &\quad + A_{1,x} h \left[\upsilon \left(\frac{W}{R} \right) - \alpha \Delta T (1+\upsilon) - (1-\upsilon) \varepsilon_{11}^t - \upsilon \varepsilon_{22}^t - \upsilon \varepsilon_{33}^t \right] \\ &\quad + A_{1,y} h [-(1-2\upsilon) \varepsilon_{12}^t] = 0 \end{aligned} \tag{28}$$

$$\begin{aligned} &\frac{\partial \mathrm{N_{s\theta}}}{\partial \mathrm{s}} + \frac{1}{\mathrm{s}} \frac{\partial \mathrm{N_\theta}}{\partial \varphi} + \frac{2\mathrm{N_{s\theta}}}{\mathrm{s}} A_1 h \left[\upsilon \frac{\partial \varepsilon_{11}^t}{\partial y} + (1-\upsilon) \frac{\partial \varepsilon_{22}^t}{\partial y} + \upsilon \frac{\partial \varepsilon_{33}^t}{\partial y} + (1-2\upsilon) \frac{\partial \varepsilon_{12}^t}{\partial x} \right] \\ &\quad + A_{1,x} h [-(1-2\upsilon) \varepsilon_{12}^t] \\ &\quad + A_{1,y} h \left[-(1-\upsilon) \left(\frac{W}{R} \right) - \alpha \Delta T (1+\upsilon) - \upsilon \varepsilon_{11}^t - (1-2\upsilon) \varepsilon_{22}^t \right. \\ &\quad \left. - \upsilon \varepsilon_{33}^t \right] \end{aligned} \tag{29}$$

$$\frac{\partial^2 \mathrm{M_s}}{\partial s^2}+\frac{2}{\mathrm{s}}\frac{\partial \mathrm{M_s}}{\partial \mathrm{s}}+\frac{2}{\mathrm{s}}\frac{\partial^2 \mathrm{M_{s\theta}}}{\partial \mathrm{s}\,\partial\varphi}-\frac{1}{\mathrm{s}}\frac{\partial \mathrm{M_\theta}}{\partial \mathrm{s}}+\frac{2}{\mathrm{s}^2}\frac{\partial \mathrm{M_{s\theta}}}{\partial\varphi}+\frac{1}{\mathrm{s}^2}\frac{\partial^2 \mathrm{M_\theta}}{\partial\varphi^2}+\frac{\mathrm{N_\theta}}{\mathrm{s}}\cot(\alpha)$$
$$=\rho \mathrm{h}\left(\frac{\partial^2 \mathrm{w}}{\partial \mathrm{t}^2}+2\mathrm{V_c(t)}\frac{\partial^2 \mathrm{w}}{\partial \mathrm{t}\,\partial \mathrm{s}}+\left(\mathrm{V_c(t)}\right)^2\frac{\partial^2 \mathrm{w}}{\partial \mathrm{s}^2}+\frac{\partial \mathrm{V_c(t)}}{\partial \mathrm{t}}\frac{\partial \mathrm{w}}{\partial \mathrm{s}}\right)$$
$$+\frac{A_1 h(1-\upsilon)\alpha\Delta T}{R}+\frac{A_1 h}{R}[\upsilon\varepsilon_{11}^t-(1-\upsilon)\varepsilon_{22}^t-\upsilon\varepsilon_{33}^t] \tag{30}$$
$$-A_{1,xx}\left(\frac{h^3(1-\upsilon)}{12}\frac{\partial^2 w}{\partial x^2}+\frac{h^3(\upsilon)}{12}\frac{\partial^2 w}{\partial y^2}\right)$$
$$-A_{1,yy}\left(\frac{h^3(1-\upsilon)}{12}\frac{\partial^2 w}{\partial y^2}+\frac{h^3(\upsilon)}{12}\frac{\partial^2 w}{\partial x^2}\right)-\frac{A_{1,xy}h^3(1-2\upsilon)}{6}\frac{\partial^2 w}{\partial y\partial x}$$

Due to the symmetrical nature and boundary conditions of the axially movable rotating cylindrical shell:

$$\delta u(x,0,z)=\delta u(x,2\pi,z) \tag{31}$$

$$\delta v(x,0,z)=\delta v(x,2\pi,z) \tag{32}$$

$$\delta w(x,0,z)=\delta w(x,2\pi,z) \tag{33}$$

$$\delta u(L,\theta,z)-\delta u(0,\theta,z)=0 \tag{34}$$

$$\delta v(L,\theta,z)-\delta v(0,\theta,z)=0 \tag{35}$$

$$\delta w(L,\theta,z)-\delta w(0,\theta,z)=0 \tag{36}$$

The zero of the axial moment and circumferential displacement are the boundary condition for simply-supported axially moving truncated conical shells.

$$M_s=0\ \&\ v=0 \qquad at\ \ s=s_1,s_2 \tag{37}$$

Besides, u,v and w must be continuous at θ. Therefore, the continuity conditions along the circumferential direction must be satisfied.

$$\int_0^{2\pi}\int_{s_1}^{s_2} N_s\,dxRd\theta=0 \tag{38}$$

$$\int_0^{2\pi}\int_{s_1}^{s_2}\frac{\partial v}{R\partial\theta}\,dsRd\theta=\int_0^{L}[v(x,2\pi)-v(x,0)]\,ds \tag{39}$$

$$\int_0^{2\pi}\int_{s_1}^{s_2} N_{s\theta}\,dsRd\theta=0 \tag{40}$$

Where ε_{ij}^{t} are components of transformation strain tensor and $A_1 = \frac{E(\eta)}{(1+\upsilon)(1-2\upsilon)}$ in which υ is Poisson's ration and E is the Young's modulus ($E = E^A + \eta(E^M - E^A)$). In order to consider the natural frequencies of the shell, the pure austenite phase was only studied. Consequently, all transformation strain components vanished because of zero martensitic volume fractions. In addition, in this article all transformation strain component and martensitic volume fraction were supposed to be dependent to stress and are independed to x, y.
The compatibility strain equation of the truncated cone shell is expressed as follows [41]:

$$\frac{\cot(\alpha)}{\mathrm{s}}\frac{\partial^2 \mathrm{w}}{\partial \mathrm{s}^2} - \frac{1}{\mathrm{s}}\frac{\partial^2 \mathrm{e}_{s\theta}}{\partial \mathrm{s}\,\partial\varphi} - \frac{1}{\mathrm{s}^2}\frac{\partial \mathrm{e}_{s\theta}}{\partial\varphi} + \frac{\partial^2 \mathrm{e}_{\theta}}{\partial \mathrm{s}^2} + \frac{1}{\mathrm{s}^2}\frac{\partial^2 \mathrm{e}_{\mathrm{s}}}{\partial\varphi^2} + \frac{2}{\mathrm{s}}\frac{\partial \mathrm{e}_{\theta}}{\partial \mathrm{s}} - \frac{1}{\mathrm{s}}\frac{\partial \mathrm{e}_{\mathrm{s}}}{\partial \mathrm{s}} = 0 \tag{41}$$

The Airy stress function used by Sofiyev in order to reduce the three nonhomogeneous partial differential equations in relations (28)-(30) to compatibility and motion equation in the radial directions is [40]:

$$(\mathrm{N}_1, \mathrm{N}_2, \mathrm{N}_{12}) = \left(\frac{1}{\mathrm{s}^2}\frac{\partial^2 \emptyset}{\partial\varphi^2} + \frac{1}{\mathrm{s}}\frac{\partial \emptyset}{\partial \mathrm{s}}\,, \frac{\partial^2 \emptyset}{\partial \mathrm{s}^2}, -\frac{1}{\mathrm{s}}\frac{\partial^2 \emptyset}{\partial \mathrm{s}\,\partial\varphi} + \frac{1}{\mathrm{s}^2}\frac{\partial \emptyset}{\partial\varphi}\right) \tag{42}$$

After substitution of airy stress function, equation (42) into the equation (41) together with equation (30), and using the variable $s = Se^x, \emptyset = \emptyset 1 e^{2x}$, the governing equations of motion are obtained as follows:

$$\begin{aligned}
&\left(\frac{\partial^2 \emptyset}{\partial x^2} + 3\frac{\partial \emptyset}{\partial x} + 2\emptyset\right) S_1 e^{3x}\cot(\alpha) \\
&\quad + \left(\frac{h^3 E(\eta)}{12(\mu^2-1)}\right)\left(\frac{\partial^4 w}{\partial\varphi^4} + \frac{\partial^4 w}{\partial x^4} - 4\frac{\partial^3 w}{\partial x^3} + 4\frac{\partial^2 w}{\partial x^2} + 2\frac{\partial^2 w}{\partial\varphi^2}\right) \\
&\quad - 2\left(\left(\frac{-h^3\mu E(\eta)}{12(\mu^2-1)}\right) + \left(\frac{h^3 E(\eta)}{12(\mu+1)}\right)\right) \\
&\quad \times \left(\frac{\partial^4 w}{\partial\varphi^2\partial x^2} - 2\frac{\partial^3 w}{\partial\varphi^2\partial x} + \frac{\partial^2 w}{\partial\varphi^2}\right) \\
&\quad - \rho h\left(\frac{\partial^2 w}{\partial t^2} + \frac{2V_c(t)}{S_1 e^x}\frac{\partial^2 w}{\partial x\partial t} + \frac{\left(V_c(t)\right)^2}{{S_1}^2 e^{2x}}\frac{\partial^2 w}{\partial x^2}\right. \\
&\quad \left. + \frac{1}{S_1 e^x}\left(\frac{d}{dt}V_c(t)\right)\frac{\partial w}{\partial x}\right) = 0
\end{aligned} \tag{43}$$

$$\begin{aligned}
&\left(\frac{1}{E(\eta)h}\right) e^{2x}\left(\frac{\partial^4 \emptyset}{\partial x^4} + 4\frac{\partial^3 \emptyset}{\partial x^3} + 4\frac{\partial^2 \emptyset}{\partial x^2} + \frac{\partial^4 \emptyset}{\partial\varphi^4} + 2\frac{\partial^2 \emptyset}{\partial\varphi^2}\right) \\
&\quad + 2\left(\left(\frac{1+\mu}{E(\eta)h}\right) - \left(\frac{\mu}{E(\eta)h}\right)\right) e^{2x} \times \left(\frac{\partial^4 \emptyset}{\partial\varphi^2\partial x^2} + 2\frac{\partial^3 \emptyset}{\partial\varphi^2\partial x} + \frac{\partial^2 \emptyset}{\partial\varphi^2}\right) \\
&\quad + \left(\frac{\partial^2 w}{\partial x^2} - \frac{\partial w}{\partial x}\right) S_1 e^x \cot(\alpha) = 0
\end{aligned} \tag{44}$$

4 Solution of the problem

We have expanded the equation of the flexural W by using the linear axisymmetric and symmetric modes. Assuming that the truncated conical shell is simply supported at both ends, the transverse displacement would be in the form of a triangular function, $w(x,\varphi,t) = \sum_{m=1}^{M} \mathrm{A_{m,n}(t)}\cos(\beta\varphi)\sin(\lambda_m x) + \mathrm{B_{m,n}(t)}\sin(\beta\varphi)\sin(\lambda_m x)$, where $\mathrm{A_{m,n}}$ is the unknown amplitude of the displacement, $\mathrm{B_{m,n}(t)}$ is the companion mode of the fundamental mode, $\mathrm{A_{m,n}}$ is the driven mode, and $\lambda_m = \frac{m\pi}{L}$ substitution "w" in the equation of (44) would be resulted in:

$$\begin{aligned}\emptyset 1 = &\left(\left((e^{-x}C4 + C2)\cos(\lambda_1 x) + (e^{-x}C3 + C1)\sin(\lambda_1 x)\right)B_1(t)\sin\left(\beta_2(\varphi)\right)\right) + \\ &\left(\left((e^{-x}C8 + C6)\cos(\lambda_2 x) + (e^{-x}C7 + C5)\sin(\lambda_2 x)\right)B_2(t)\sin\left(\beta_2(\varphi)\right)\right)\end{aligned} \tag{45}$$

The coefficient is calculated by Maple software. After substituting w and equations (45) into equation (43) and applying the Galerkin method with convenient weighting factors, the equation with the appropriate function is applied:

$$\begin{aligned}Z_s(x,\theta) &= sin\left(\frac{(s+1)\pi x}{2L}\right)cos(n\theta)\,; s = Odd\ ,\ Z_s(x,\theta) \\ &= sin\left(\frac{(s)\pi x}{2L}\right)sin(n\theta);\ s = even\end{aligned} \tag{46}$$

After integration and some rearrangements, the governing equations will be written as:

$$\frac{d^2}{dt^2}\left(B_{1,n}\right) + B_1\frac{d}{dt}\left(B_{1,n}\right) + B_2\frac{d}{dt}\left(B_{2,n}\right) + B_3B_{1,n} + B_4B_{2,n} = 0 \tag{47}$$

$$\frac{d^2}{dt^2}\left(A_{1,n}\right) + B_1\frac{d}{dt}\left(A_{1,n}\right) + B_2\frac{d}{dt}\left(A_{2,n}\right) + B_3A_{1,n} + B_4A_{2,n} = 0 \tag{48}$$

We can find an approximate solution by using the multiple scales method. By introducing new independent variables $T_0 = \tau$ and $T_1 = \varepsilon\tau$ the form of the solution of equations (47), and (48) are as follows:

$$B_i(\tau,\varepsilon) = B_i^0(T_0,T_1) + \varepsilon B_i^1(T_0,T_1) + O(\varepsilon^2), i = 1,2 \tag{49}$$

The first and second derivative of equation (49) can be written as:

$$\dot{B}_i = \frac{\partial}{\partial T_0}B_i^0 + \varepsilon\left(\frac{\partial}{\partial T_1}B_i^0 + \frac{\partial}{\partial T_0}B_i^1\right) + \varepsilon^2\frac{\partial}{\partial T_1}B_i^1\ , i = 1,2 \tag{50}$$

$$\ddot{B}_i = \frac{\partial^2}{\partial {T_0}^2}B_i^0 + \varepsilon\left(2\frac{\partial}{\partial T_1}\frac{\partial}{\partial T_0}B_i^0 + \frac{\partial^2}{\partial {T_0}^2}B_i^1\right) + \varepsilon^2\left(2\frac{\partial}{\partial T_1}\frac{\partial}{\partial T_0}B_i^1 + \frac{\partial^2}{\partial {T_0}^2}B_i^0\right), i = 1,2 \tag{51}$$

By substituting $V(t) = V_0 + \varepsilon V_1 \cos(\Omega\tau)$ into the equations (50), (51), and separating terms for order 0, we can write:

$$\frac{\partial^2}{\partial {T_0}^2} B_1^0 + a_{11} \frac{\partial}{\partial T_0} B_2^0 + (b_{11} V_0^2 + b_{12}) B_1^0 = 0 \tag{52}$$

$$\frac{\partial^2}{\partial {T_0}^2} B_2^0 - a_{11} \frac{\partial}{\partial T_0} B_1^0 + (b_{21} V_0^2 + b_{22}) B_2^0 = 0 \tag{53}$$

By casting the equations (52), (53) into the matrix form:

$$\mathrm{M}\begin{pmatrix} \ddot{B}_1^{(0)} \\ \ddot{B}_2^{(0)} \end{pmatrix} + \mathrm{C}\begin{pmatrix} \dot{B}_1^{(0)} \\ \dot{B}_2^{(0)} \end{pmatrix} + \begin{pmatrix} B_1^{(0)} \\ B_2^{(0)} \end{pmatrix} = \begin{pmatrix} 0 \\ 0 \end{pmatrix} \tag{54}$$

The solution of order ε^0 has the following exponential form:

$$\begin{pmatrix} B_1^{(0)} & B_2^{(0)} \end{pmatrix} = \Psi e^{\lambda\tau} \quad \Longrightarrow \quad \left|\lambda^2 M + \lambda C + K\right| = 0 \tag{55}$$

Where λ implies the eigenvalues of the above matrix and can be written in the form of $\lambda = \xi + i\omega$, while its real part is zero when the rotational speed is below the critical speed. Hence it can be written as, $\lambda = i\omega$, and the natural frequencies ω_1 and ω_2 satisfy eq. (56),

$$\omega^4 - \left(\beta_1 + \beta_2 + a_{11}^2\right)\omega^2 + \beta_1\beta_2 = 0 \tag{56}$$

By solving similar to what is said in Article [47] the natural frequency ω_1, ω_2 are as bellows:

$$\omega_1 = \sqrt{\frac{(\beta_1 + \beta_2 + a_{11}^2) + \sqrt{(\beta_1 + \beta_2 + a_{11}^2)^2 - 4\beta_1\beta_2}}{2}} \tag{57}$$

$$\omega_2 = \sqrt{\frac{(\beta_1 + \beta_2 + a_{11}^2) - \sqrt{(\beta_1 + \beta_2 + a_{11}^2)^2 - 4\beta_1\beta_2}}{2}} \tag{58}$$

5 Numerical results and discussion

5.1 Validation

In order to compare the results obtained from the equations derived in this paper and their solution method with the results of previous works, first, the two cases presented in the work of [42] are investigated. The first case involves a very long cylindrical shell under rotating conditions, and the second is the case of a nonrotating cylindrical shell presented in the work of [18]. The specifications of the material are listed in Table (1).

Table (2) can be employed to compare the value of the natural frequency of modes (1,2) to (1,6) with ref. [42]. Due to the simplification assumptions of the shallow Donnell shell, such as ignoring shear deformation and in-plane inertia, the accuracy of the natural frequency depends on the number of circular waves (n). when ($\frac{1}{n^2} \ll 1$) The accuracy is acceptable.

Strangely, it depends on the number of circular waves selected; it can be observed in Table (1), where the results converge to (n≥4). The results can be compared to those of an axially moving circular cylindrical shell. By the consideration of zero value for the cone angle, the conical shell structures could be converted to a cylindrical shell so that the results can be compared with the previous studies on an axially moving cylindrical shell. Table (3) shows the value of the natural frequency of modes (1,3) and (1,5) with ref. [18]. Also our study are validated with the one whose vibrations analysis was performed on smart alloys state by [38] . They utilized DQM to calculate the natural frequencies of the thin-walled cylindrical shell in their study and solved them analytically. We also solve the same shell, using the proposed formulation. The outcomes and their comparison with the results of [38] are predicted in Fig. (4).

Table 1 Material parameters of Ni-Ti SMA

Material parameter	value	Material parameter	value
H	0.056	$\rho(\mathrm{kg/m^3})$	6448.1
A_s(k)	307.5	E^A(GPa)	67
A_f(k)	322	E^M(GPa)	26.3
M_s(k)	291.4	$\alpha(\mathrm{k^{-1}})$	22e-6
M_f(k)	282	C^A(J/kg k)	13.8
υ(k)	0.3	C^M(J/kg k)	8
σ_s^{cr}	100(Mpa)	σ_f^{cr}	170(Mpa)

Table 2 Comparison of the natural dimensionless frequency parameter $\mathrm{f} = \omega \mathrm{R}_2 \sqrt[2]{\frac{(1-\mu^2)\rho}{\mathrm{E}}}$ for an infinitely long nonrotating isotropic conical shell ($\frac{h}{R_2} = 0.01, \frac{Lsin(\alpha)}{R_2} = 0.25$)

n	$\alpha = 30^0$		
	Lam and Hua [42]	Present work	Error(%)
2	0.8420	0.8447	0.3
3	0.7376	0.7363	0.17
4	0.6362	0.6352	0.15
5	0.5528	0.5538	0.15
6	0.4950	0.4953	0.06

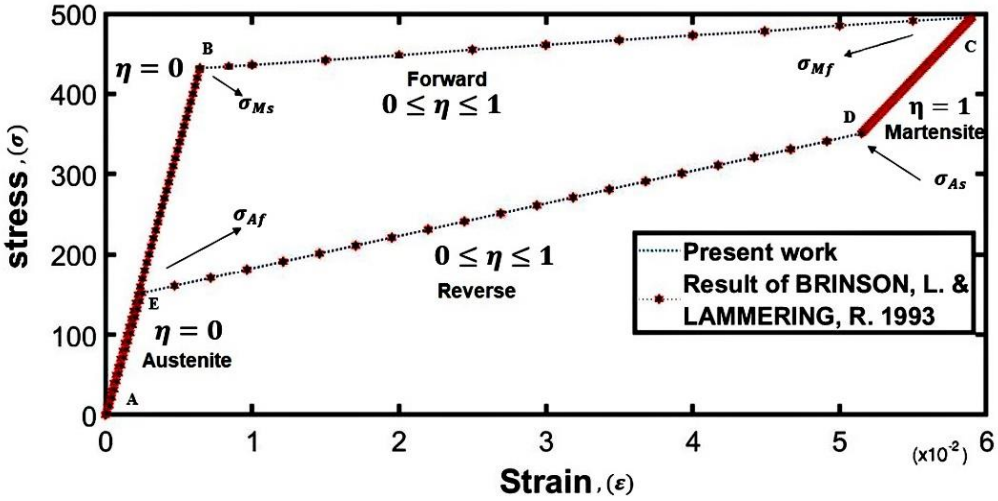

Figure 3 Stress-strain diagram of pseudoelastic SMA for the 1D case at $T = 328k$

Table 3 Comparison of the natural frequency of an axially moving cylindrical shell ($\frac{h}{R} = 0.0247, \frac{L}{R} = 2$)

n	V	Mohamadi, Shahgholi [18]	Present work	Error (%)
3	0	1727.28	1727.12	0.0092
	400	1264.81	1264.65	0.012
	800	0	0	0
5	0	739.24	739.27	0.004
	400	0	0	0
	800	1540.15	1540.13	0.0012

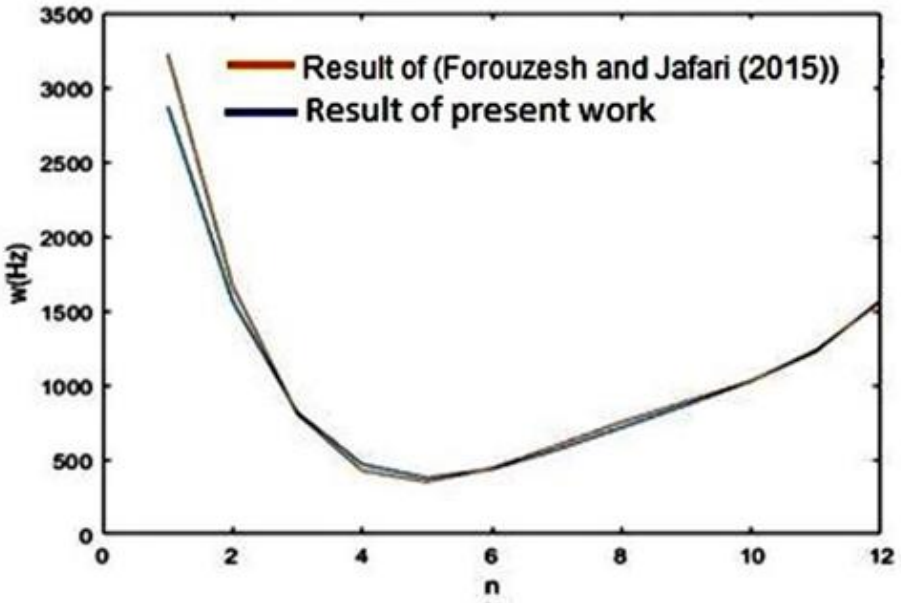

Figure 4 Comparison of the natural frequency w.r.t. circumferential wave number in pure austenite phase and first axial mode (m=1) obtained from the present methodology and that of Forouzesh and Jafari [38]

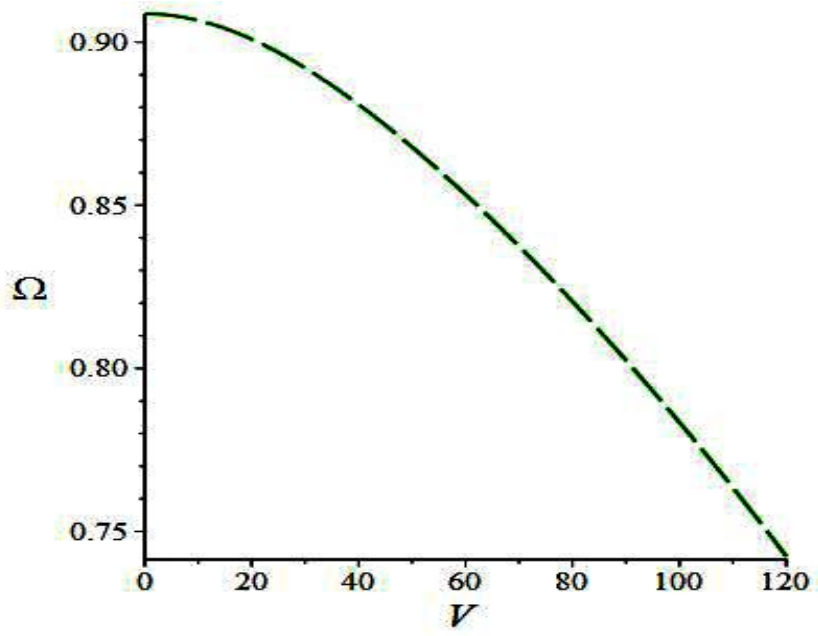

Figure 5 Natural frequency Vs. velocity of axially moving truncated conical shell in pure austenite phase $T = 328k$

5.2 Results and discussion

In the present study, first, as shown in Figure (5), the effect of axial velocity of the structure on the natural frequency in the absence of excitation and damping force is investigated. The results show that the natural frequency of the incomplete conical shell decreases with increasing axial velocity. As compared with which one in the [47] that made ordinary alloy steel, it can be understood that the natural frequency of SMA truncated conical shell reaches zero at a lower axial velocity.

The results of numerical research and drawing of real and imaginary parts of the frequency response show that there are two types of instability in the axially moving conical shell. One is divergence instability and the other is flutter instability. Therefore, the stability or instability of an axially moving truncated conical shell can be investigated. As can be seen in figure (6), if the axial velocity of the structure is zero, the real part of the eigenvalue will be zero, and the imaginary value of the eigenvalue, which represents the natural frequency of the system, will be nonzero. Adding the axial velocity to the structure will cause changes in eigenvalues. The real part of the eigenvalue decreases with increasing the velocity. This reduction continues until the system's natural frequency converges to zero. At this point, the first instability occurs in the system. This kind of in- stability is divergent instability, and the axial velocity at this point is the critical velocity. When the velocity reaches the critical point, the real part of the eigenvalue has two values; therefore, static instability, bifurcation occurs at this point. As the velocity increases relative to the critical velocity, the imaginary part of the eigenvalue is still zero, but a change occurs in the actual eigenvalue. These changes continue as the velocity increases until both branches of the real part of the eigenvalue converge to zero. At this point, both the real and imaginary parts of the eigenvalue are zero. Now, increasing the velocity changes the imaginary part of the eigenvalue and increases the natural frequency of the system. In addition, the real part of the eigenvalue does not change with increasing the velocity and remains at zero. In fact, the system regains its stability at this point. Then, an increase in the axial velocity results in a stage where the real part of the eigenvalue changes and bifurcation occurs again. Indeed, the second instability, dynamic instability, flutter, occurs for the system at this velocity [43]. The results of the study of other movable axial structures such as beams [44] plates [45] and axially moving cylindrical shells [18],[46] also show the same thing. As compared with which one in the [47] that made ordinary alloy steel, it can be understood that the instability point, i.e., Flutter and Bifurcation point of axially moving SMA truncated conical shell reaches zero at lower axial velocity.

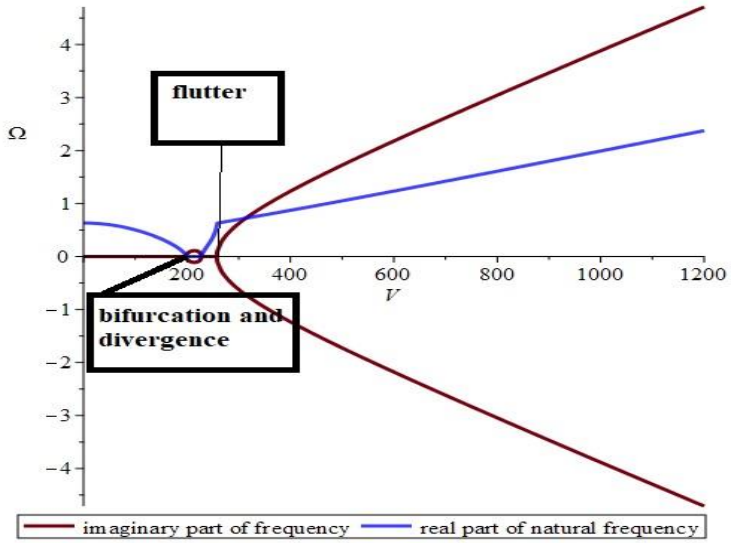

Figure 6 Changes in real and imaginary parts of the frequency at different speeds in pure austenite phase $T = 328k$

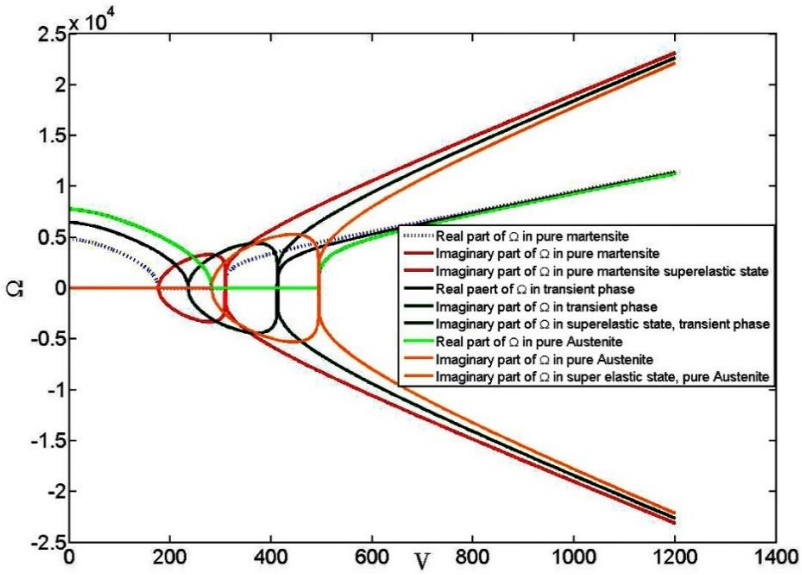

Figure 7 Changes in real and imaginary parts of the frequency at different speeds and different phase

Figure (7) shows the changes in real and imaginary parts of natural frequency by changing the value of axial velocity and the effect of phase transformation. As can be seen, the frequency response of the system shifts to the left, in another word the divergence and flutter occurs at lower axial velocity due to the material staying in a transient state or pure martensite phase. Figure 8(a) shows the effect of the velocity on the imaginary parts of eigenvalues $m = 2$ and $n =$ 1,2,3,6. The first point to consider in this form is the frequency change of the structure in the static case. In this mode, when the system axial velocity is zero, the natural frequency of the system decreases with increasing circumferential wave numbers. Moreover, notable is the divergence instability points. With increasing circumferential wave numbers, the divergence instability occurs at lower velocities. Other checkable tips are the natural frequency changes at very high velocities. The difference of the natural frequency changes of the system for different circumferential wave numbers is small at very high velocities so that the natural frequency of the system increases for different circumferential wave numbers to converge with increasing the velocity. Figure 8(b) shows the effect of the velocity on the real parts of eigenvalues for $m = 2$ and n = 1,2,3,6. As can be seen, values of critical and flutter velocities decrease for different circumferential wave numbers from low to higher modes. For different modes, the difference between the critical velocities is not very large, but the difference in the amount of the velocity is very high at the flutter point. Therefore, the point of divergence instability is not very different for various modes, but the velocity of the flutter point is very different with increasing the circumferential wavenumbers, and the flutter instability for lower circumferential wave numbers occurs at much higher velocities than higher circumferential wave numbers. It should be noted that the results in Figures 8(a) and 8(b) are for the conical shell with a cone angle of 30°. In the following, various results are observed for different cone angles, and the influence of the cone angle will change these results.

When the angle of the cone is zero, the structure turns into a cylindrical shell, in which case the change in natural frequency in the number of different half-waves modes is negligible. As can be seen, the imaginary part of the frequency diagram is shown in Figure (9) in terms of axial velocity at different angles. As the angle of the cone increases, the natural frequency of the system first increases. The natural frequency also increases and then decreases with increasing cone angle and axial velocity. This increase and decrease of frequency up to an angle of 63 degrees have similar results for different ambient half-waves. But at an angle of 63 degrees, the

effect of different modes on frequency changes will be minimal, and we will have a relatively constant frequency for different modes, which is approximately convergent in the diagram. When this quantity was compared in the presence of axial speed, at first these are equal until about 13^o and after that, the natural frequency has a lower quantity. As compared with which one in the [47] that made ordinary alloy steel, it can be understood that at an angle of 63 degrees, the effect of different modes and different materials on frequency changes will be minimal, and we will have a relatively constant frequency for different modes, which is approximately convergent in the diagram.

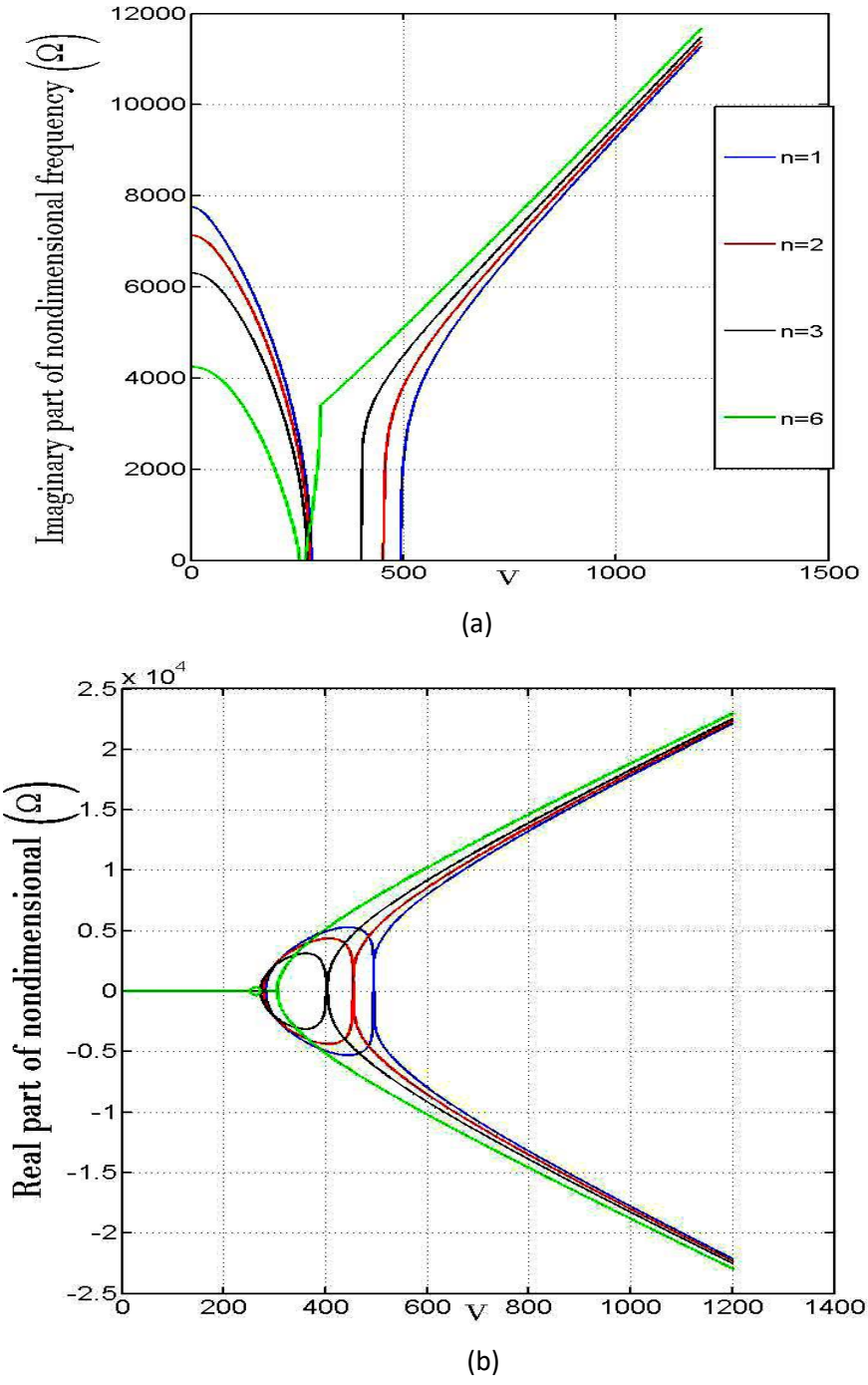

Figure 8 a) Imaginary part of nondimensional frequency at different speeds and b) Real parts of the frequency at different speeds in pure austenite phase $T = 328k$

Figure 10(a) shows the effect of the aspect ratio on the imaginary parts of eigenvalues of an axially moving conical shell, indicating that increasing the thickness and decreasing the radius will increase the natural frequency of the system. Figure 10(b) shows the effect of the aspect ratio on the real parts of eigenvalues of an axially moving conical shell, which indicates changing the instability points of the system. It means that critical and flutter points will be created at a lower velocity as the thickness decreases or the radius increases. Furthermore, the divergence instability range of the system increases by decreasing the radius or increasing the structure thickness.

In order to study the effect of apex angles on stability and instability of the conical shells, three angles were chosen i.e., $\alpha = 10, 30, 60$, and we analyzed the stability and instability of the axially moving conical shell. The stability analysis of axially moving shells has been done by plotting of the real and imaginary parts of natural frequency versus the velocity. As can be seen in the figure (11) the bifurcation critical velocity and flutter critical velocity decrease by increasing the apex angle.

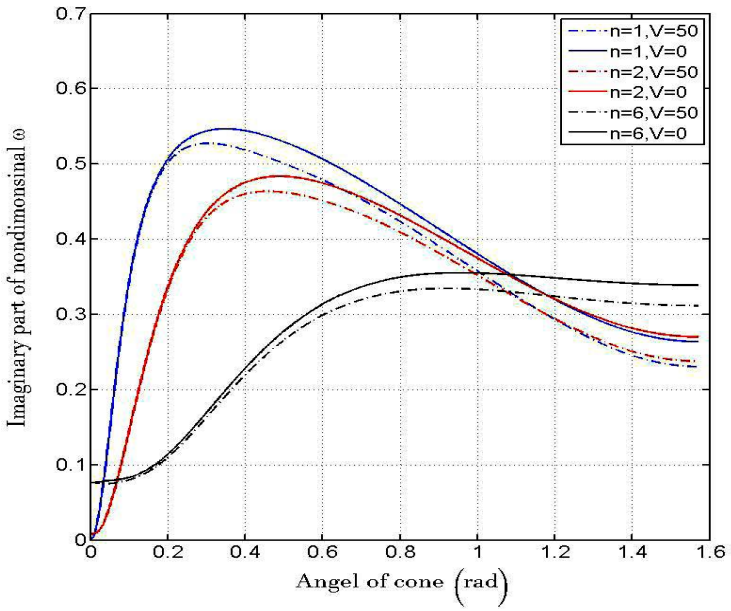

Figure 9 Imaginary parts of the frequency by changing the cone angle in pure austenite phase $T = 328k$

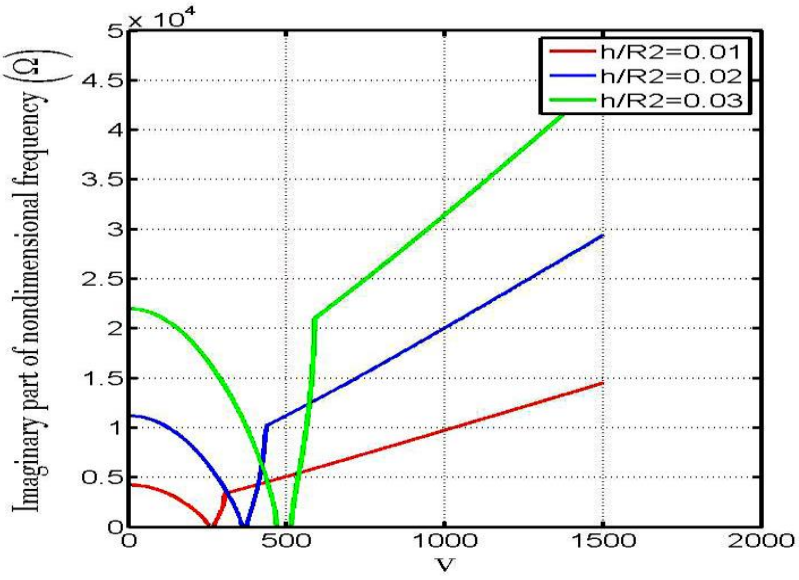

(a)

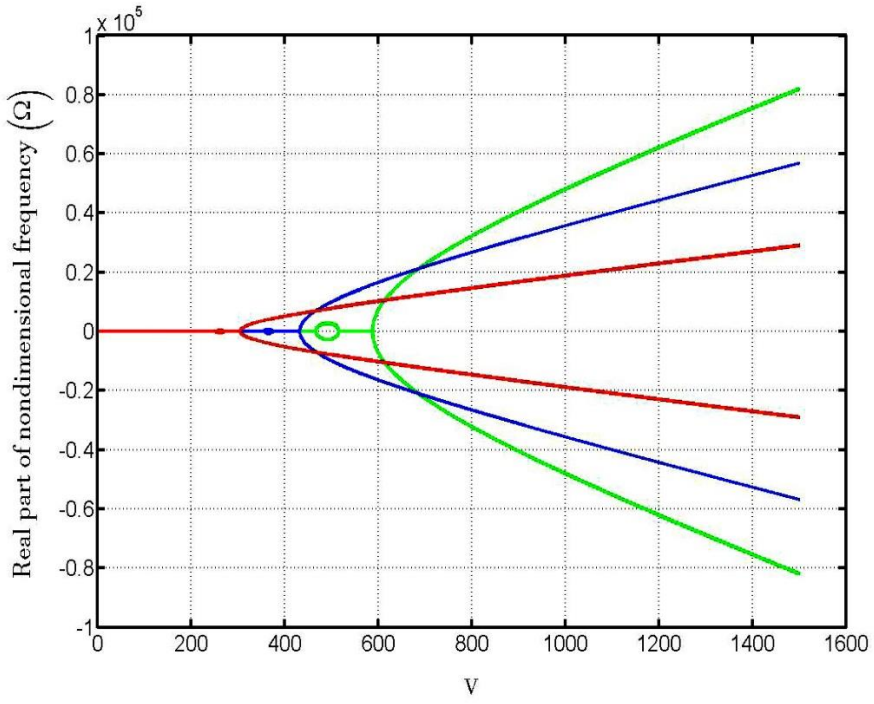

(b)

Figure 10 Real and imaginary parts of the frequency at different $\frac{h}{R}$ by changing the velocity value in pure austenite phase $T = 328k$

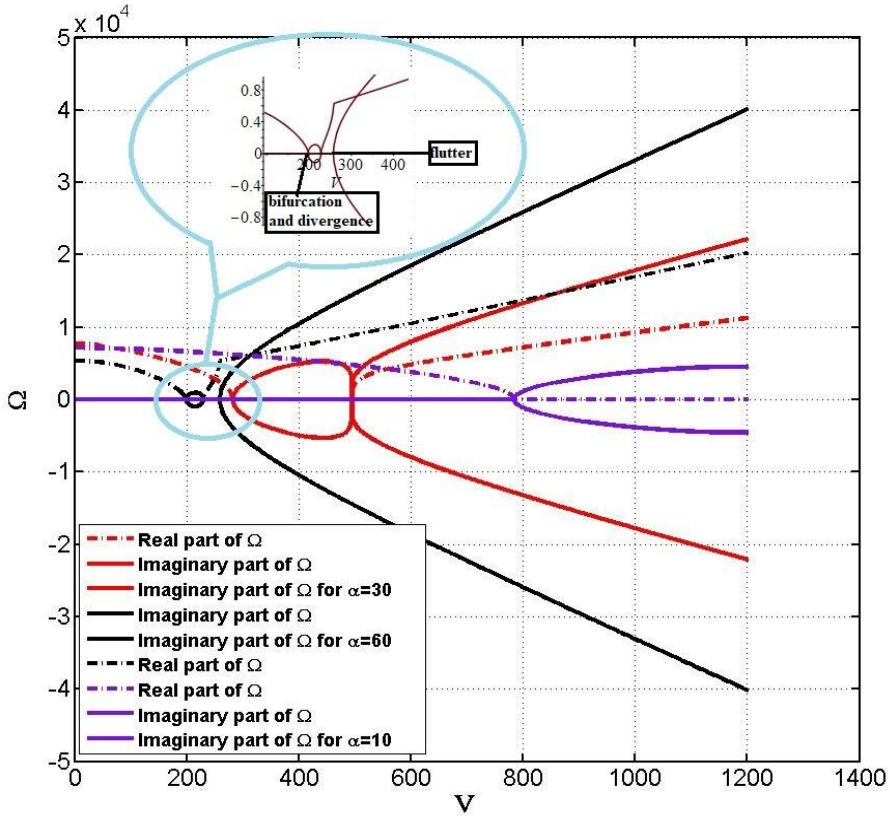

Figure 11 Real and imaginary parts of the frequency at different apex angles by changing the velocity value in pure austenite phase $T = 328k$

6 Conclusion

The vibrations of thin-walled axially moving conical shells made of shape memory alloy with simple supports were analyzed in this paper. First, the equation of motions was derived by using Hamilton's principle and convenient relations for shape memory alloy. The shell vibration analysis and its natural frequencies investigation were performed using the Galerkin method and multiple scale method. By extracting the critical velocity of the structure, the stability and instability of the system for different modes and velocities were investigated. In general, two types of instability occur in the studied structure. The first type of instability is called divergence instability and occurs when the real and imaginary parts of the frequency are both zero, and the instability of the second type is called flutter and occurs when the bifurcation phenomenon occurs in the diagram and the real part of the eigenvalues has two values. The effect of the material state on real and imaginary parts of natural frequency by changing the value of axial velocity shows that the frequency response of the system shifts to the left, in other words the divergence and flutter occurs at lower axial velocity due to the material staying in a transient state or in pure martensite/austenite phase. Increasing the apex angle of a movable conical axis shell with a constant aspect ratio creates critical points and a flutter at lower speeds. It can be seen that by increasing the angle of the cone, the distance between the critical points of the divergence and the filter changes so that by increasing the angle of the cone, this distance decreases. The amount of frequency at different angles increases with increasing axial velocity. This trend continues up to an angle of 63 degrees, and in general, at an angle of 63 degrees the effect of different modes on frequency changes will be minimal and we will have a relatively constant frequency for different modes that almost convergence occurs in the diagram. Before this angle, the imaginary part of the frequency, which represents the natural frequency of the shell, increases, and after that, its value will decrease. The normal frequency of the system increases before the 63-degree angle with increasing cone angle and then decreases.

References

[1] Brinson, L.C., "One-dimensional Constitutive Behavior of Shape Memory Alloys: Thermomechanical Derivation with Non-constant Material Functions and Redefined Martensite Internal Variable", Journal of Intelligent Material Systems and Structures, Vol. 4(2), pp. 229-242, (1993).

[2] Paiva, A., and M.A., Savi, "An Overview of Constitutive Models for Shape Memory Alloys", Mathematical Problems in Engineering, Vol. 2006, pp. 1-30, (2006).

[3] Savi, M.A., De Paula, A.S., and Lagoudas, D.C., "Numerical Investigation of an Adaptive Vibration Absorber using Shape Memory Alloys", Journal of Intelligent Material Systems and Structures, Vol. 22(1), pp. 67-80, (2011).

[4] Lagoudas, D.C., "*Shape Memory Alloys: Modeling and Engineering Applications*", 1st Edition, Springer, Texas, pp.106-166, (2010) .

[5] Tanaka, K., "A Thermomechanical Sketch of Shape Memory Effect: One-dimensional Tensile Behavior", Mechanica, Vol. 18, pp. 251-263, (1986).

[6] Tanaka, K., Kobayashi, S., and Sato, Y., "Thermomechanics of Transformation Pseudoelasticity and Shape Memory Effect in Alloys", International Journal of Plasticity, Vol. 2(1), pp. 59-72, (1986).

[7] Liang, C., and Rogers, C.A., "One-dimensional Thermomechanical Constitutive Relations for Shape Memory Materials", Journal of Intelligent Material Systems and Structures, Vol. 8(4), pp. 285-302, (1997).

[8] Bo, Z., and Lagoudas, D.C., "Thermomechanical Modeling of Polycrystalline SMAs under Cyclic Loading, Part I: Theoretical Derivations", International Journal of Engineering Science, Vol. 37(9), pp. 1089-1140, (1999).

[9] Bo, Z., and Lagoudas, D.C., "Thermomechanical Modeling of Polycrystalline SMAs under Cyclic Loading, Part IV: Modeling of Minor Hysteresis Loops", International Journal of Engineering Science, Vol. 37(9), pp. 1205-1249, (1999).

[10] Lagoudas, D.C., and Bo, Z., "Thermomechanical Modeling of Polycrystalline SMAs under Cyclic Loading, Part II: Material Characterization and Experimental Results for a Stable Transformation Cycle", International Journal of Engineering Science, Vol. 37(9), pp. 1141-1173, (1999).

[11] Bo, Z., and Lagoudas, D.C., "Thermomechanical Modeling of Polycrystalline SMAs under Cyclic Loading, Part III: Evolution of Plastic Strains and Two-way Shape Memory Effect", International Journal of Engineering Science, Vol. 37(9), pp. 1175-1203, (1999).

[12] Leclercq, S., and Lexcellent, C., "A General Macroscopic Description of the Thermomechanical Behavior of Shape Memory Alloys", Journal of the Mechanics and Physics of Solids, Vol. 44(6), pp. 953-980, (1996).

[13] Helm, D., and Haupt, P., "Shape Memory Behaviour: Modelling within Continuum Thermomechanics", International Journal of Solids and Structures, Vol. 40(4), pp. 827-849, (2003).

[14] Civalek, Ö., "An Efficient Method for Free Vibration Analysis of Rotating Truncated Conical Shells", International Journal of Pressure Vessels and Piping, Vol. 83(1), pp. 1-12, (2006).

[15] Chen, C., and Dai, L., "Nonlinear Vibration and Stability of a Rotary Truncated Conical Shell with Intercoupling of High and Low Order Modals", Communications in Nonlinear Science and Numerical Simulation, Vol. 14(1), pp. 254-269, (2009).

[16] Sofiyev, A., "The Non-linear Vibration of FGM Truncated Conical Shells", Composite Structures, Vol. 94(7), pp. 2237-2245, (2012).

[17] Chen, Y., Zhao, H.B., Shen, Z.p., Grieger, I., and Kröplin, B.H., "Vibrations of High Speed Rotating Shells with Calculations for Cylindrical Shells", Journal of Sound and Vibration, Vol. 160(1), pp. 137-160, (1993).

[18] Mohamadi, A., Shahgholi, M., and Ghasemi, F.A., "Free Vibration and Stability of an Axially Moving Thin Circular Cylindrical Shell using Multiple Scales Method", Meccanica, Vol. 54(14), pp. 2227-2246, (2019).

[19] Hua, L., "Influence of Boundary Conditions on the Free Vibrations of Rotating Truncated Circular Multi-layered Conical Shells", Composites Part B: Engineering, Vol. 31(4), pp. 265-275, (2000).

[20] Lam, K., and Hua, L., "Influence of Boundary Conditions on the Frequency Characteristics of a Rotating Truncated Circular Conical Shell", Journal of Sound and Vibration, Vol. 223(2), pp. 171-195, (1999).

[21] Hua, L., "Frequency Characteristics of a Rotating Truncated Circular Layered Conical Shell", Composite Structures, Vol. 50(1), pp. 59-68, (2000).

[22] Abolhassanpour, H., Ashenai Ghasem, F., and Mohamadi, A., "Stability and Vibration Analysis of an Axially Moving Thin Walled Conical Shell", Journal of Vibration and Control, Vol. 28(13-14), pp. 1-18, (2021).

[23] Wang, Y., Guo, X.H., Chang, H.H., and Li, H.Y., "Nonlinear Dynamic Response of Rotating Circular Cylindrical Shells with Precession of Vibrating Shape—Part I: Numerical Solution", International Journal of Mechanical Sciences, Vol. 52(9), pp. 1217-1224, (2010).

[24] Sarkheil, S., and Foumani, M.S. .,"An Improvement to Motion Equations of Rotating Truncated Conical Shells", European Journal of Mechanics-A/Solids, Vol. 62, pp. 110-120, (2017).

[25] Wang, Y., Ding, H., and Chen, LQ., "Vibration of Axially Moving Hyperelastic Beam with Finite Deformation", Applied Mathematical Modelling, Vol. 71, pp. 269-285, (2019).

[26] Sofiyev, A., and Pancar, E., "The Effect of Heterogeneity on the Parametric Instability of Axially Excited Orthotropic Conical Shells", Thin-Walled Structures, Vol. 115, pp. 240-246, (2017).

[27] Shin, C., Chung, J., and Kim, W., "Dynamic Characteristics of the Out-of-plane Vibration for an Axially Moving Membrane", Journal of Sound and Vibration, Vol. 286(4-5), pp. 1019-1031, (2005).

[28] Najafov, A., Sofiyev, A., and Ozyigit, P., "Vibration and Stability of Axially Compressed Truncated Conical Shells with Functionally Graded Middle Layer Surrounded by Elastic Medium", Journal of Vibration and Control, Vol. 20(2), pp. 303-320, (2014).

[29] Anh, V.T.T., and Duc, N.D., "Vibration and Nonlinear Dynamic Response of Eccentrically Stiffened Functionally Graded Composite Truncated Conical Shells Surrounded by an Elastic Medium in Thermal Environments", ACTA Mechanica, Vol. 230(1), pp. 157-178, (2019).

[30] Kerboua, Y., Lakis, A., and Hmila, M., "Vibration Analysis of Truncated Conical Shells Subjected to Flowing Fluid", Applied Mathematical Modelling, Vol. 34(3), pp. 791-809, (2010).

[31] Sofiyev, A., "On the Vibration and Stability Behaviors of Heterogeneous-CNTRC-Truncated Conical Shells under Axial Load in the Context of FSDT", Thin-Walled Structures, Vol. 151, pp. 106747, (2020).

[32] Shokrollahi, H., "Effect of Vertex Angle on Elastic-plastic Stability of a Steel Open Conical Shell", Journal of Solid Mechanics, Vol. 12(4), pp. 791-803, (2020).

[33] Avey, M., Fantuzzi, N., and Sofiyev, A., "Thermoelastic Stability of CNT Patterned Conical Shells under Thermal Loading in the Framework of Shear Deformation Theory", Mechanics of Advanced Materials and Structures, Vol. 29, pp. 1-14, (2022).

[34] Kazemi, M., Kouchakzadeh, M., and Shakouri, M., "Stability Analysis of Generally Laminated Conical Shells with Variable Thickness under Axial Compression", Mechanics of Advanced Materials and Structures, Vol. 27(16), pp. 1373-1386, (2020).

[35] Zamani, M., and Heydari Beni, M., "Transient Dynamic Analysis of Grid-stiffened Composite Conical Shells", Journal of Solid Mechanics, Vol. 14(3), pp. 312-331, (2021).

[36] Nekouei, M., Raghebi, M., and Mohammadi, M., "Free Vibration Analysis of Laminated Composite Conical Shells Reinforced with Shape Memory Alloy Fibers", ACTA Mechanica, Vol. 230(12), pp. 4235-4255, (2019).

[37] Xu, L., Solomou, A., Baxevanis,T., and Lagoudas, D., "A Three-dimensional Constitutive Modeling for Shape Memory Alloys Considering Two-way Shape Memory Effect and Transformation-induced Plasticity", Report AIAA, Grant Number: NNX17AJ96A, (2018).

[38] Forouzesh, F., and Jafari, A.A., "Radial Vibration Analysis of Pseudoelastic Shape Memory Alloy Thin Cylindrical Shells by the Differential Quadrature Method", Thin-Walled Structures, Vol. 93, pp. 158-168, (2015).

[39] Amabili, M., "*Nonlinear Vibrations and Stability of Shells and Plates*", 1st Edition, Cambridge University Press, London, United Kingdom, pp. 90-119, (2008).

[40] Sofiyev, A., and Kuruoglu, N., "Non-linear Buckling of an FGM Truncated Conical Shell Surrounded by an Elastic Medium", International Journal of Pressure Vessels and Piping, Vol. 107, pp. 38-49, (2013).

[41] Sofiyev, A., "Non-linear Buckling Behavior of FGM Truncated Conical Shells Subjected to Axial Load", International Journal of Non-Linear Mechanics, Vol. 46(5), pp. 711-719, (2011).

[42] Lam, K., and Hua, L., "Vibration Analysis of a Rotating Truncated Circular Conical Shell", International Journal of Solids and Structures, Vol. 34(17), pp. 2183-2197, (1997).

[43] Banichuk, N., Jeronen, J., Neittaanmäki, P., Saksa, T., and Tuovinen, T., "*Mechanics of Moving Materials*", 2rd Edition, Finland, Springer, pp. 30-61, (2014).

[44] Hai-Wei, LV., Liang, Li., and Ying-Hui, Li., "Non-linearly Parametric Resonances of an Axially Moving Viscoelastic Sandwich Beam with Time-dependent Velocity", Applied Mathematical Modelling, Vol. 53, pp. 83-105, (2018).

[45] Wang, Y., Cao, X., Jing, T., and Wu, J., "Dynamic Characteristics and Stability of Axially Moving Viscoelastic Plate with Piezoelectric Layer", Journal of Low Frequency Noise, Vibration and Active Control, Vol. 33(3), pp. 341-355, (2014).

[46] Abolhassanpour, H., Shahgholi, M., Ashenai Ghasemi, F., and Mohammadi, A., "Nonlinear Vibration Analysis of an Axially Moving Thin-walled Conical Shell", International Journal of Non-Linear Mechanics, Vol. 134, pp. 103747, (2021).

[47] Vahidi, H., Shahgholi, M., Rahmani Hanzaki, A., and Mohammadi, A., "Effect of Angle and Axiall Velocity on Natural Frequency and Stability of Axially Moving Truncated Conical Shell", The 29th International Conference of the Iranian Association of Mechanical Engineers, ISME2021-IC1462, Tehran, Iran, (2021).

Nomenclature

A_f: Austenite finish

A_s: Austenite starts

C_A, C_M: Relation between temperature and critical stress

$E^{SMA}(E, \gamma, T)$: The modulus of the shape memory alloy

E^A: Amount of memory alloy in state of complete austenite

E^M: Amount of memory alloy in state of complete martensite

M_f: Martensite finish

M_s: Martensite start

η: Fraction of the martensite

Ω: Dimensionless fluctuation frequency

σ_θ, σ_r: Stress in θ, r direction

ε^t: Transformation strain

Appendix A

In this portion, the relation of SMA that is mentioned in section 1 is given.

$$b^A = -\Delta s_0\left(A_f - A_s\right),\ b^M = -\Delta s_0\left(M_s - M_f\right), \mu_1 = \frac{1}{2}\rho\Delta s_0\left(M_s + A_f\right) - \rho\Delta u_0$$

$$\mu_2 = \frac{1}{4}\rho\Delta s_0\left(A_s - A_f + M_s - M_f\right) - \rho\Delta u_0$$

$$\Lambda = \begin{cases} \frac{3}{2}H\frac{\sigma'}{\bar{\sigma}'},\ \dot{\eta} > 0 \\ H\frac{\varepsilon^t}{\bar{\varepsilon}_t},\ \dot{\eta} < 0 \end{cases}$$

$$\bar{\sigma} = \left(\frac{3}{2}\sigma' : \sigma'\right)^{\frac{1}{2}} = \left(\frac{3}{2} \parallel \sigma' \parallel^2\right)^{\frac{1}{2}}$$

$$\bar{\varepsilon^t} = \left(\frac{2}{3}\varepsilon^t : \varepsilon^t\right)^{\frac{1}{2}} = \left(\frac{3}{2} \parallel \varepsilon^t \parallel^2\right)^{\frac{1}{2}}$$

$$Y = \frac{1}{4}\rho\Delta s_0\left(M_s + M_f - A_s - A_f\right)$$

$$\Delta\varepsilon_{q+1}^{t\ k} = \Delta\eta_{q+1}^k \Lambda_{q+1}^k$$

$$\Delta\sigma_{q+1}^{t\ k} = -\Delta\eta_{q+1}^k S_{q+1}^{k\ -1} : \left(\begin{cases} \partial_\sigma\phi_{q+1}^k,\ \dot{\eta} > 0 \\ -\partial_\sigma\phi_{q+1}^k,\ \dot{\eta} < 0 \end{cases}\right)$$

$$\phi_{q+1}^k + \partial_\sigma\phi_{q+1}^k : \Delta\sigma_{q+1}^k + \partial_\eta\phi_{q+1}^k\Delta\eta_{q+1}^k = 0$$

$$\Delta\eta_{q+1}^k = \begin{cases} \frac{\phi_{q+1}^k}{\partial_\sigma\phi_{q+1}^k : \mathrm{D}_{q+1}^k : \partial_\sigma\phi_{q+1}^k - \partial_\eta\phi_{q+1}^k},\ \dot{\eta} > 0 \\ \frac{-\phi_{q+1}^k}{-\partial_\sigma\phi_{q+1}^k : \mathrm{D}_{q+1}^k : \partial_\sigma\phi_{q+1}^k - \partial_\eta\phi_{q+1}^k},\ \dot{\eta} < 0 \end{cases}$$

$$\varepsilon_{q+1}^{t(k+1)} = \varepsilon_{q+1}^{t\ k} + \Delta\varepsilon_{q+1}^{t\ k}$$

$$\eta_{q+1}^{t(k+1)} = \eta_{q+1}^{t\ k} + \Delta\eta_{q+1}^{t\ k}$$

$$\sigma_{q+1}^{t(k+1)} = \sigma_{q+1}^{t\ k} + \Delta\sigma_{q+1}^{t\ k}$$